Journal of Radioanalytical and Nuclear Chemistry (2025) 334:6763–6772
https://doi.org/10.1007/s10967-025-10266-0

# Sedimentation rate and chronology of Çınarcık Basin, the Marmara Sea

İ. Koraltan[1] · İ. Sert[2] · N. İ. Elek[2] · B. Oluçay[2] · O. Güven[3] · S. F. Özmen[4] · G. Yaprak[2] · M. Yücel[5]

Received: 16 January 2025 / Accepted: 3 July 2025 / Published online: 20 September 2025


## Abstract

The Çınarcık Basin, the deepest point of the sea at 1270 m, is an important area for the accumulation and preservation of sediments and serves a natural archive for environmental change. In this study, unlike previous studies, short-term sedimentation trends in the basin are presented for the last century. To establish a reliable $^{210}$Pb chronology, CRS and CIC Models were applied to process the $^{210}$Pb data and validation was done from records of fallout $^{137}$Cs. Models CRS and CIC were used because the profile distribution of lead does not decay exponentially. The mean sedimentation rates obtained from $^{210}$Pb dating were calculated as 0.36 cmy$^{-1}$ (CRS) and 0.39 cmy$^{-1}$ (CIC). $^{137}$Cs dating indicated rates of 0.39 cmy$^{-1}$ at 14 cm depth (1986) and 0.33 cmy$^{-1}$ at 19 cm depth (1963). In parallel with the developing industry in the region, sediment accumulation rates have shown an increasing trend in the last three decades.

**Keywords** Çınarcık Basin sediment · Anthropogenic impact · CRS–CIC models · Marine ecosystem · Recent sedimentation · $^{210}$Pb · $^{137}$Cs

## Introduction

The Marmara Sea is characterized by a layered water structure where water masses from the Black Sea and the Mediterranean interact. Waters from the Aegean Sea flow in through the Dardanelles, while those from the Black Sea enter via the Bosphorus, influencing the sea's temperature and salinity distribution. These currents are important factors affecting the accumulation processes of sediments on the seabed and the dynamics of the ecosystem [1–3].

Surrounding the sea is the Marmara watershed Türkiye's most densely populated and industrialized region. The sea also holds strategic geopolitical value as a critical node in international maritime transportation. Despite its historical ecological richness, the Marmara Seas marine environment has experienced significant decline in recent decades [4]. Given its ecological and economic importance, numerous national projects have been initiated to promote sustainable management and environmental protection. These efforts have addressed a wide range of issues, including tectonics, sedimentation, biodiversity, microplastics, pollution monitoring, and maritime logistics [5].

The foundation for long-term monitoring was laid with the "National Marine Measurement and Monitoring Program Marmara Sea Sub-Project" (1989–1997), followed by the "Marmara Sea Integrated Modelling System (MARMOD)" (2017–2023). Since 2017, the "Integrated Marine Pollution Monitoring Programme" has provided regular assessments of chemical and ecological quality, focusing on pollution levels and anthropogenic pressures.

The Sea of Marmara has been also a significant focus of paleoceanographic research; geological structure, tectonics [6–9] and sedimentology [10–14]. Within this context, the Çınarcık Basin serving as a key site for the accumulation and preservation of organic-rich sediments, represents a valuable natural archive for studying environmental change [2, 3, 15, 16]. While earlier studies in Çınarcık

✉ İ. Sert
ilker.sert@ege.edu.tr

1 Institute of Natural and Applied Sciences, Akdeniz University, 07070 Antalya, Turkey

2 Institute of Nuclear Sciences, Ege University, 35100 İzmir, Turkey

3 Faculty of Fisheries, Akdeniz University, 07070 Antalya, Turkey

4 Vocational School of Technical Sciences, Akdeniz University, 07070 Antalya, Turkey

5 Institute of Marine Sciences, Middle East Technical University, 33731 Mersin, Turkey

Basin [1, 17] provided valuable insights into long-term tectono-seismic and diagenetic processes through accelerator mass spectrometry, radiocarbon ($^{14}$C, half-life: 5730 years) dating and geochemical analyses, high resolution reconstructions of short-term sedimentation trends particularly over the past century remain limited.

To reconstruct recent sedimentation history, natural and artificial radioactive isotopes such as lead-210 ($^{210}$Pb, half-life: 22.30 years) and caesium-137 ($^{137}$Cs, half-life: 30.14 years) are commonly used. These isotopes act as temporal markers, allowing for accurate dating of sediment layers. $^{14}$C dating is valuable for long-term environmental reconstructions spanning tens of thousands of years [18–20], whereas $^{210}$Pb and $^{137}$Cs are better suited for short-term sedimentation rate analysis over the past 100–150 years [21–23]. In particular, $^{210}$Pb part of the uranium-238 ($^{238}$U, half-life: $4.47 \times 10^9$ years) decay series is extensively used to estimate recent accumulation rates, while $^{137}$Cs, a fallout product from nuclear testing, provides an independent time marker that strengthens chronological accuracy [24–26].

Under conditions of uniform sediment accumulation, the vertical profile of non-equilibrium (atmospheric) $^{210}Pb_{excess}$ ($^{210}Pb_{ex}$) within sediment cores exhibits an exponential pattern, which is fundamental for sediment dating. However, variations in the vertical distribution of.$^{210}Pb_{ex}$ can arise due to fluctuations in accumulation rates over time, differences in the physical structure of the sediments, and the influence of physical and biological mixing processes [27]. Specifically, changes in sediment supply driven by increased fluvial input from intensified precipitation, sea-level variations, or anthropogenic influences such as deforestation and land-use changes can alter accumulation dynamics. Furthermore, bioturbation by benthic fauna and physical disturbances including sediment resuspension induced by storms, slumping events, or surface erosion can redistribute 21$^{0}$Pbex within the sediment column, thereby obscuring its expected exponential distribution [28–32]

To determine sedimentation rates using $^{210}Pb_{ex}$, three primary models are applied: the Constant Flux (CF) and Constant Sedimentation (CS) model (CF and CS model), the Constant Rate of Supply (CRS) model, and the Constant Initial Concentration (CIC) model [21, 33]. The selection of model depends on the accuracy of the sampling, the study region, and the profile distribution of $^{210}Pb_{ex}$ [34–37]. According to Gökmen et al., 1996, the sedimentation rates were 0.19 and 0.073 g cm$^{-2}$ y$^{-1}$ at the shelves of Bosporus and the Dardanelles and between 0.055 and 0.064 g cm$^{-2}$ y$^{-1}$ in northern part of the Sea of Marmara [38]. Ergin et al., 1992 determined the sedimentation rate as 0.28 cm y$^{-1}$ in the southwestern shelf of the Sea of Marmara [39]. In this study, unlike the previous studies, short-term sedimentation trends in the basin are presented for the last hundred years.

The aim of this study is to explore the sedimentation history of the Marmara Sea over the past century by analysing the radioisotopes $^{137}$Cs and $^{210}$Pb in the Çınarcık Basin. The distinguishing feature of this study from monitoring studies is the use of radioanalytical techniques for sediment analysis. These findings will enhance understanding of the region's environmental history and shifts in the marine ecosystem, while also providing a valuable basis for assessing historical anthropogenic impacts through the compilation of data from previous monitoring projects and research articles, thereby enabling new and comprehensive environmental evaluations.

## Material and methods

Sediment core sample were collected from a depth of 1,270 m (40.7772 N; 28.87974 E) during sea expeditions conducted aboard the R/V Bilim-2 in June 2022, a research vessel operated by the Middle East Technical University, Institute of Marine Sciences Fig. 1.

Sediment cores were collected using an Oktopus-Kiel multi-corer sampler equipped with tubes measuring 10 cm in diameter and 60 cm in length. The samples were carefully transported to the ship laboratory, maintaining their original sediment profile. After visual documentation, the cores were cut into 1 cm-thick and preserved at −20 °C for radionuclide analysis. The samples were then transferred to the Ege University, Institute of Nuclear Science for further processing.

For analysis, the sediment slices were placed in an oven to dry at 45 °C for 8–10 days and homogenized using a Retsch RM 200 grinding mortar. Each sediment sample (15 g) was compressed into a pellet with a diameter of 40 mm and a thickness of 6 mm. A hydraulic press was used to apply a pressure of 200 kg cm⁻2 to form the pellets. No additives were incorporated into the sediment during processing. The samples were sealed under the vacuum and then stored for at least 25 days to ensure the secular equilibrium radium-226 ($^{226}$Ra, half-life: 1600 years) and its decay products before the gamma spectrometry measurements.

In order to measure sediment particle sizes, samples were collected throughout the core, mixed with pure water using a DLAB OS20-S mechanical mixer, and were not pre-treated. No additional fillers or dispersants have been used. Grain size distribution was examined using a Mastersizer 3000 laser analyzer. This method can measure particles ranging from 0.01 to 3500 µm in a single analysis. Each sample was analysed in three replicates to ensure accuracy and reproducibility. Laser diffraction offers a rapid, efficient approach with minimal sample requirements and a broad measurement range, making it highly effective for particle size determination [40].

In this study, activity concentrations of the sediment samples were measured two HPGe gamma spectrometry

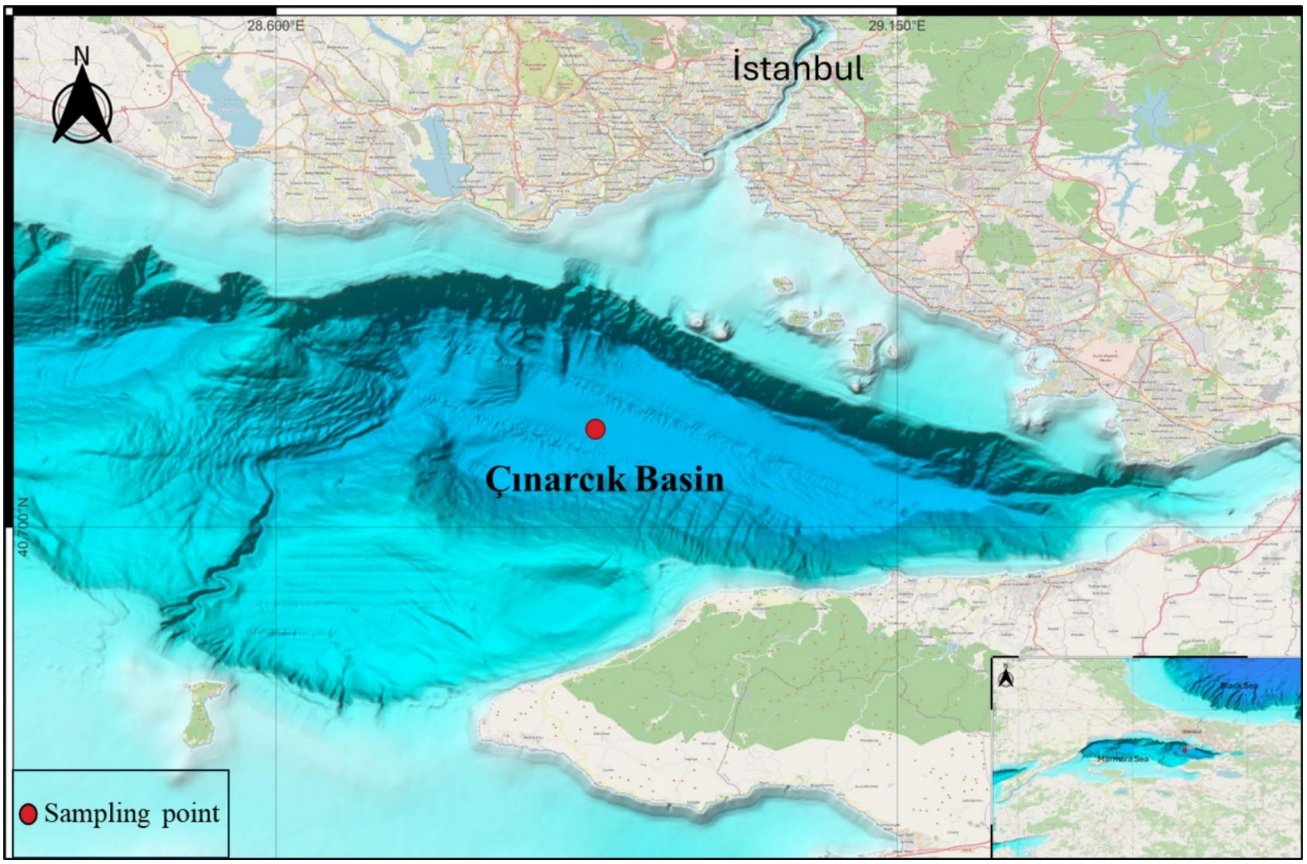


**Fig. 1** Study area of sediment core in Çınarcık Basin the Marmara Sea

systems. The measurement of $^{210}$Pb in the samples was performed by ORTEC planar HPGe low energy photon detectors (FWHM = 0.585 keV at 122 keV with a 0.25 mm beryllium (Be) window) with related electronics connected to a PC-based multichannel analyser and the associated software. The detector is shielded by 100 mm thick lead bricks internally lined with 1.5 mm copper foil. The ORTEC GLP Series Planar Low-Energy Photon Spectrometer (LEPS) is for use in applications over the energy range from 3 to ~ 300 keV and has a lower background with $1.12\times10^{-3}$ counts/sec for 46.5 keV gamma line of $^{210}$Pb.

A 184 cm$^3$ p-type coaxial HPGe detector with a relative efficiency of 25% and a resolution of 1.85 keV at 1.332 MeV (with associated electronics procured from EG&G Ortec) was employed for the measurement of potassium-40 ($^{40}$K, half-life: $1.25\times10^9$ years), $^{226}$Ra, thorium-232 ($^{232}$Th, half-life: $14.05\times10^9$ years) and $^{137}$Cs activity in the sediment samples. The detector was shielded by 100 mm thick lead bricks internally lined with 1.5 mm copper foil. The spectrum is acquired and analysed using a PC-based multichannel analyser and the associated software.

Energy and efficiency calibrations of these detectors are made according to the ASTM E 181–98 (Reapproved 2003) standards. The efficiency checks out of the systems were performed by IAEA certified; RGU-1, RGTh-1, RGK-1, IAEA-447, IAEA-410, IAEA-385, IAEA-152/156 standard reference materials with similar matrix and geometry to the samples.

The efficiency calibrations for coaxial detectors are made in the energy range between 60 keV and 3 MeV, and in the range 3- 300 keV for planar low energy HPGe detector. In all gamma spectrometric measurements of sediment samples, the activity of $^{226}$Ra was evaluated from the 1764.49 keV peak of bismuth-214 ($^{214}$Bi, half-life: 19.90 min), and $^{232}$Th activity is evaluated from the 2,614.53 keV peak of thallium-208 ($^{208}$Tl, half-life: 3.05 min) while those of $^{40}$K and $^{137}$Cs activities were determined from their characteristic gamma line of 1460.75 keV and 661.66 keV, respectively. Meanwhile, $^{210}$Pb activities of the samples were determined using peak at 46.5 keV in the low energy gamma spectrum. The Minimum Detectable Activities (MDA) depends on the background spectrum, counting time, detector size, sample properties, measurement geometry, and nuclear decay data of the considered radionuclides. The MDAs of the gamma spectrometer systems based on the Currie criteria ([2] in supplementary materials) in the case of a well-known

background for $^{226}$Ra, $^{232}$Th, $^{40}$K, $^{137}$Cs and $^{210}$Pb were estimated to be 12,12, 40, 2.5 and, 14 Bq kg$^{-1}$ respectively, for the counting time 150,000–200,000 s and a sample weight of 15 g pellet geometry. Counting times were adjusted to achieve reasonable counting statistics. The background spectra were taken for 1–2 days and used to correct the net peak areas of the related radionuclides. Uncertainty of the net peak area was given from Poisson "counting statistics. The radionuclides activity concentrations were determined with one sigma error (IAEA, 2004). Relative uncertainties of the activity measurements at 68% confidence level were usually lower than 20%. A detailed description of the method is described in supplementary materials under the heading "Measurements method".

Three models utilized for determining sedimentation rates in $^{210}$Pb dating are CF and CS, CRS, and CIC. CF and CS model assumes that the unsupported $^{210}$Pb concentrations in each layer along the core are the same and equal its initial $^{210}$Pb concentration and sediment accumulation rate are constant. In these situations, if the vertical distribution of unsupported $^{210}$Pb activity concentrations shows exponential decay and thus the CF and CF model will give reliable chronology [37]. The CRS model is better suited for scenarios where the profile distribution of unsupported $^{210}$Pb concentrations shows a non-monotonic decrease due to the sediment content (As is known, each sediment layer may not have the same grain size, which affects the radionuclide retention in the sediment layers. Therefore, the radionuclide distribution along the core will not be in the form of exponential decay but in the form of deviations from exponentiality.) and specific geological conditions [37]. The monotonic decline with depth in unsupported $^{210}$Pb concentration, and in sediment cores that obtained from same area, the total cumulative residual unsupported $^{210}$Pb concentrations vary proportionally with the mean sediment accumulation rate, CIC model will give the reliable chronology [41].

## Results and discussion

Average sediment density throughout the sediment core from Çınarcık Basin is $2.32 \pm 0.2$ g cm$^{-3}$, ranging from 2.05 g cm$^{-3}$ to 2.71 g cm$^{-3}$. Especially in the CRS model, sediment densities are an important parameter in determining the total $^{210}$Pb inventory and atmospheric $^{210}$Pb flux through the sediment core. During periods of no rainfall, the amount of clay and silt accumulated in the sediment increases, which increases the retention of $^{210}$Pb in the sedimentary material and reduces the sediment accumulation rate. In this respect, grain size analysis is another important parameter. According to the analysis results, silt fraction dominated sediment particulate pool throughout the core Fig. 2.

Porosity smoothly decreased from 0.828 to 0.707 in core. It shows only one peak at seventeenth layer (0.994) and this layer had the highest sedimentation rate. In general, there is no successive increase and decrease in porosity. It shows a consistent value throughout the core profile, indicating that the sediment structure consists of particles with the same grain size.

Athy (1930) and Begy et. al. (2009) argue that the profile distribution of porosity typically shows an exponential

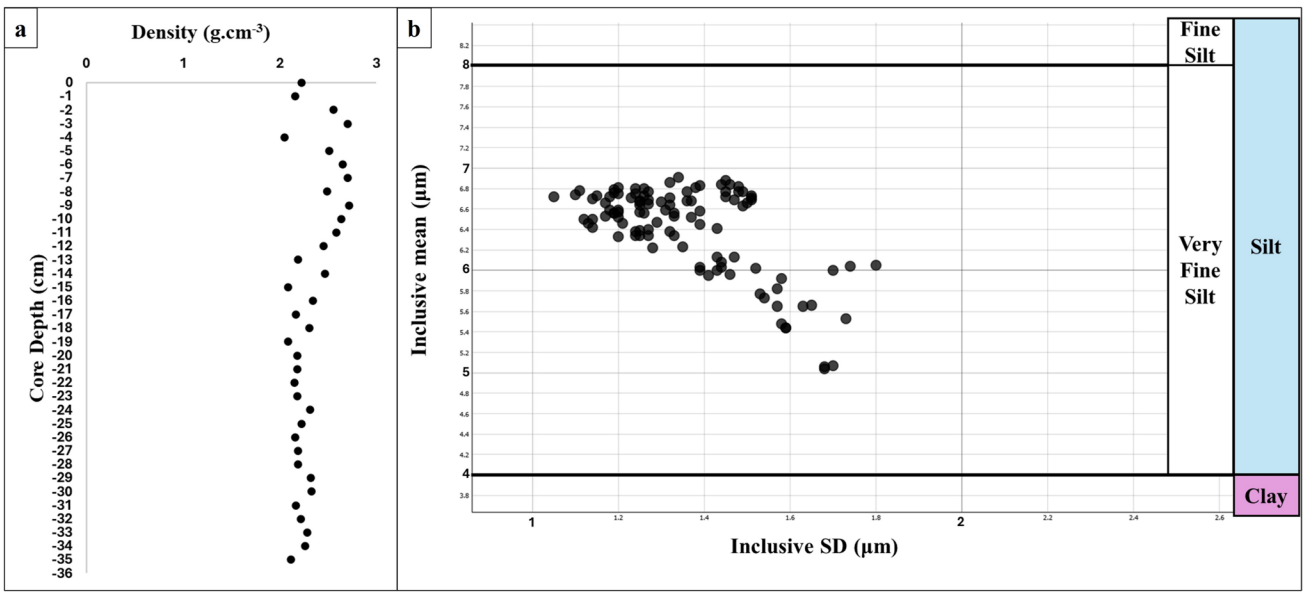


**Fig. 2** **a** Density and **b** grain size distribution of the core

decrease with depth in homogeneous sediments that experience uniform compaction [42, 43]. Contrary Klump calculated the fifteen porosity profiles in eastern Lake Superior and they showed a non-exponential decrease with depth in porosity profile [44] and findings were explained as: A wide variety of materials, from sand to clay, organic to inorganic, accumulate in deep sea and lake sediments. However, physical and environmental factors such as bottom currents, water temperature and residence time of the sedimentary particles in the water column play an active role on sediment porosity. In addition to physical and environmental effects, chemical effects such as remineralization of dissolved inorganic carbon, ammonium and oxygen in the sediment pore water also determine sediment porosity. By Sert et al. (2016) calculated four profiles in Lake Bafa and they pointed out that profiles exhibited different character from each other according to location that has different accumulation materials inside of the lake [45]. In this study, porosity has not displayed exponential decrease along the sediment profile.

Vertical distribution of unsupported $^{210}$Pb ($^{210}Pb_{ex}$) activity concentrations varies between $76.4 \pm 7.2$ and $10.1 \pm 1.7$ Bq kg$^{-1}$ along the core. Max unsupported $^{210}$Pb concentration is higher than those the North Aegean Sea ($66.6 \pm 6.1$ Bq kg$^{-1}$) [39], Mumbai Harbour Bay ($37 \pm 10.8$ Bq kg$^{-1}$) [46] and is lower than Gülbahçe Bay ($107.9 \pm 4.6$ Bq kg$^{-1}$) [37]. In a similar way, profile distribution of $^{226}$Ra activity concentration ranges from $25.0 \pm 4.8$ to $11.0 \pm 3.5$ Bq kg$^{-1}$ in the core. Max $^{226}$Ra activity is higher than those the Gülbahçe Bay ($21.0 \pm 2.0$ Bq kg$^{-1}$), Mumbai Harbour Bay ($11.2 \pm 3.0$ Bq kg$^{-1}$) and is lower than the North Aegean Sea ($40.6 \pm 4.1$ Bq kg$^{-1}$). In sediment cores, $^{226}$Ra activity is known as supported $^{210}$Pb activity. Consequently, the unsupported $^{210}$Pb activity is determined by subtracting the $^{226}$Ra activity from the total $^{210}$Pb activity in each layer. Thus, the determination of dating relies on the utilization of unsupported $^{210}$Pb activities.

When glimpsed to the vertical distribution of $^{210}Pb_{ex}$ activity concentrations Fig. 4 it is observed that they do not follow the expected exponential decrease from the top to the bottom of the core. Therefore, rather than the CF and CF model, the CRS and CIC models were used to reach a reliable chronology.

Sedimentation rate ranges from $0.58 \pm 0.04$ to $0.10 \pm 0.01$ cm y$^{-1}$ for CRS model and from $0.54 \pm 0.03$ to $0.11 \pm 0.01$ cm y$^{-1}$ for CIC model along the core, Illustrating the upward trend over the timescale from the 1910s to the present day. The trend of sedimentation rate displays two peaks at third ($0.81 \pm 0.07$ cm y$^{-1}$) and eleventh ($1.06 \pm 0.15$ cm y$^{-1}$) levels from sediment surface observed corresponding to 2017 and 1996 years respectively. In these years, it is thought that the increase in sediment accumulation may be due to extreme weather events such as heavy rainfall and flooding. Since, during periods of heavy rainfall, the amount of sand accumulated in the sediment increases, which reduces the adhesion of $^{210}$Pb in the sedimentary material and increases the rate of sediment accumulation. Vertical distribution of the sedimentation rate along the core can be investigated in three Sects. (1, 2, 3). Sect. 1 consists of the first six levels from the top of the core. Sect. 2 contains the next eight levels, while Sect. 3 encompasses the lower portion of the core. The lowest sedimentation rates are found in Sect. 4, which corresponds to time scale between 1914 and 1963. Sedimentation rates in the second section are higher than the first one and it corresponds to time interval between 1971 and 2007 years. The third section has the highest sedimentation rates and it corresponds to time interval from 2011 to sampling year (2022). The sampling point has a core depth of 29 cm, which corresponds to a timescale of 110 years. Core inventory was determined as $3263 \pm 57$ mBq cm$^{-2}$ so $^{210}$Pb flux was also calculated as 101.5 mBq cm$^{-2}$ y$^{-1}$. Determined core inventory is higher than those the north Aegean sea ($7809 \pm 88$ Bq m$^{-2}$) [41], Gülbahçe Bay ($665 \pm 26$ mBq cm$^{-2}$), Lake Bafa ($683 \pm 26$ mBq cm$^{-2}$) [45], Lake Karagöl ($724 \pm 27$ mBq cm$^{-2}$) [47].

Known atmospheric $^{210}$Pb flux values around the world start from $15.8 \pm 11.3$ mBq cm$^{-2}$ y$^{-1}$ in north 0–10 latitudes and reach to $2.0 \pm 1.5$ mBq cm$^{-2}$ y$^{-1}$ in north 70–80 latitudes and it starts from 11.7 mBq cm$^{-2}$ y$^{-1}$ in south 0–10 latitudes decreases to $0.2 \pm 0.1$ mBq cm$^{-2}$ y$^{-1}$ in south 80–90 latitudes [29]. The Sea of Marmara is between 39–42 north latitudes and average atmospheric $^{210}$Pb flux of the world is $15.5 \pm 7.5$ mBq cm$^{-2}$ y$^{-1}$ in this area. It is likely that calculated $^{210}$Pb flux value for the Sea of Marmara exceeds the global average value of atmospheric levels for the corresponding site. This elevated flux cannot be explained by atmospheric deposition alone, indicating additional sources of $^{210}$Pb input from the surrounding catchment area. These inputs are most likely driven by soil erosion resulting from intensified human activities such as rapid urbanization, coastal development, industrialization, and the expansion of agriculture in the Marmara region, particularly since the late twentieth century [48–50]. Furthermore, increasing frequencies of extreme weather events such as heavy rainfall and flooding, possibly linked to climate change have likely enhanced surface runoff and riverine transport of terrestrial material into the basin [49, 51, 52]. Altogether, these findings emphasize the significant influence of both anthropogenic and climatic factors on sediment dynamics in the Sea of Marmara.

Our sedimentation rates for the Marmara Sea are higher than the ones in north Aegean Sea ($0.399 \pm 0.011$–$0.032 \pm 0.001$ cm y$^{-1}$) [41], Lake Bafa ($0.185 \pm 0.007$–$0.042 \pm 0.005$ cm y$^{-1}$), and are roughly same with Lake Karagöl ($0.5718 \pm 0.039$–$0.044 \pm 0.002$ cm y$^{-1}$) [45], and are lower than the Thermaikos Gulf in Eastern

Mediterranean ($0.88 \pm 0.15$, $0.75 \pm 0.06$ cm $y^{-1}$ max values of the two cores) [53] and Golden Horn Estuary (1 cm $y^{-1}$) [54].

The vertical distributions of $^{137}Cs$, $^{226}Ra$ and $^{210}Pb_{ex}$ activity concentrations are shown in the Figs. 3 and 4 $^{137}Cs$ activity remained below MDA at depths below 25 cm. The peak of $^{137}Cs$ activity at 14 cm depth with a value of $8.11 \pm 2.43$ Bq $kg^{-1}$ corresponds to the Chernobyl nuclear accident in 1986. The maximum $^{137}Cs$ activity of $11.03 \pm 4.14$ Bq $kg^{-1}$ was observed at 19 cm depth and is attributed to global precipitation from atmospheric nuclear weapon tests, with the peak occurring in 1963. Based on these data, the sedimentation rate was estimated as 0.39 cm $y^{-1}$ for 1986 at 14 cm depth and 0.33 cm $y^{-1}$ for 1963 at 19 cm depth.

The CRS and CIC models indicate a sedimentation rate of 0.36 cm $y^{-1}$ and 0.39 cm $y^{-1}$, respectively. Analyzing the CRS model data, we find that a depth of 13 cm corresponds to the year $1989 \pm 0.93$, while 15 cm corresponds to $1984 \pm 1.22$. Furthermore, the 19th centimeter represents the year $1963 \pm 1.81$, Fig. 5, SM Table 1. Thus, obtained chronology with $^{210}Pb$ technique (CRS and CIC models) was corrected by using independent method that was time markers (peaks of $^{137}Cs$).

## Conclusions

There are various geochronological dating methods available today, but each has a different dating period and sensitivity. For this reason, it is recommended that the chronology obtained in dating studies be checked with a different independent method or well-defined time indicators. In this study sedimentation rate, sedimentation pattern and chronology over the last century were studied by using activity concentrations of $^{210}Pb$ and $^{137}Cs$ radionuclides in mathematical models (CRS and CIC). These results provide a valuable basis for assessing historical anthropogenic pressures in the region. First, vertical distributions of radioactivity concentrations were determined by utilizing gamma spectroscopy. Second, sediment chronology was achieved for Çınarcık Basin and verified with independent technique ($^{137}Cs$). It was observed that the results obtained with both methods were compatible with each other.

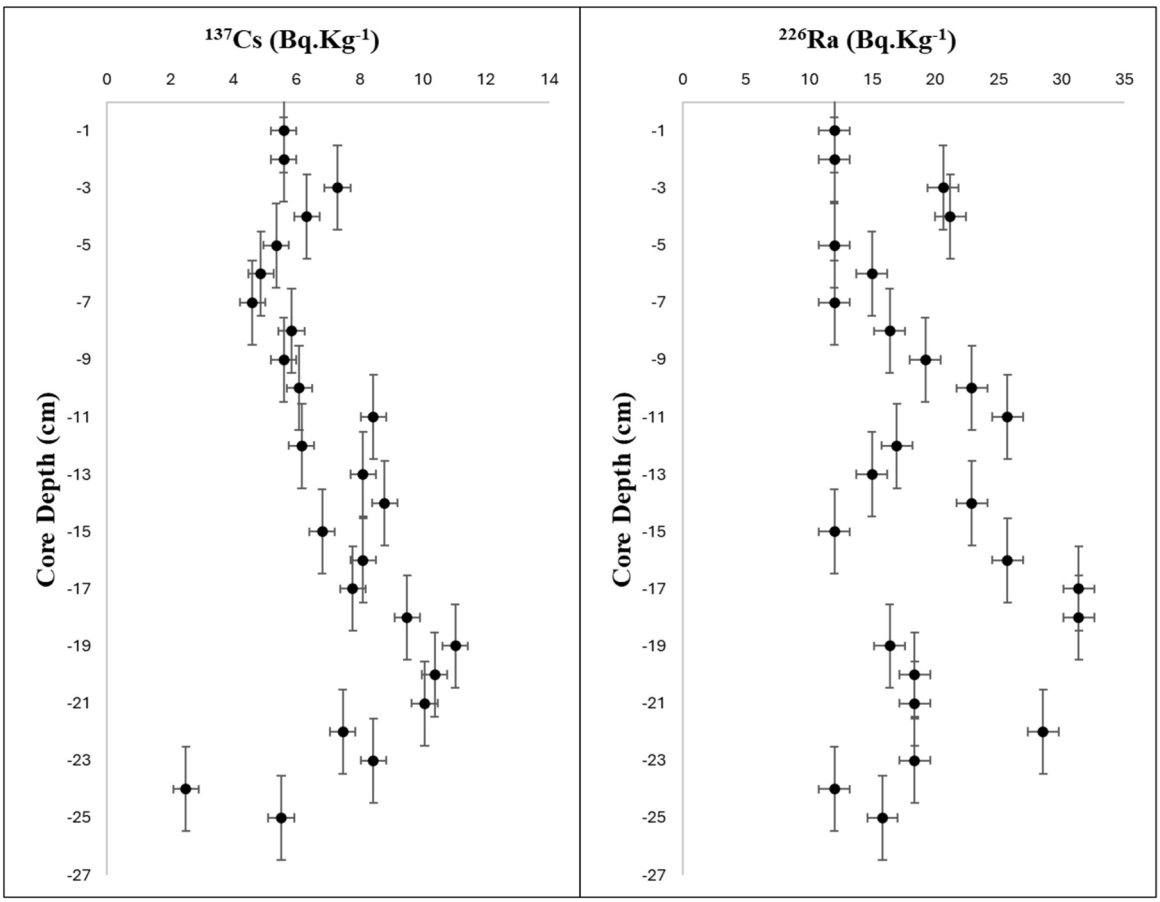


**Fig. 3** Vertical distribution of $^{137}Cs$ and $^{226}Ra$ activity in core

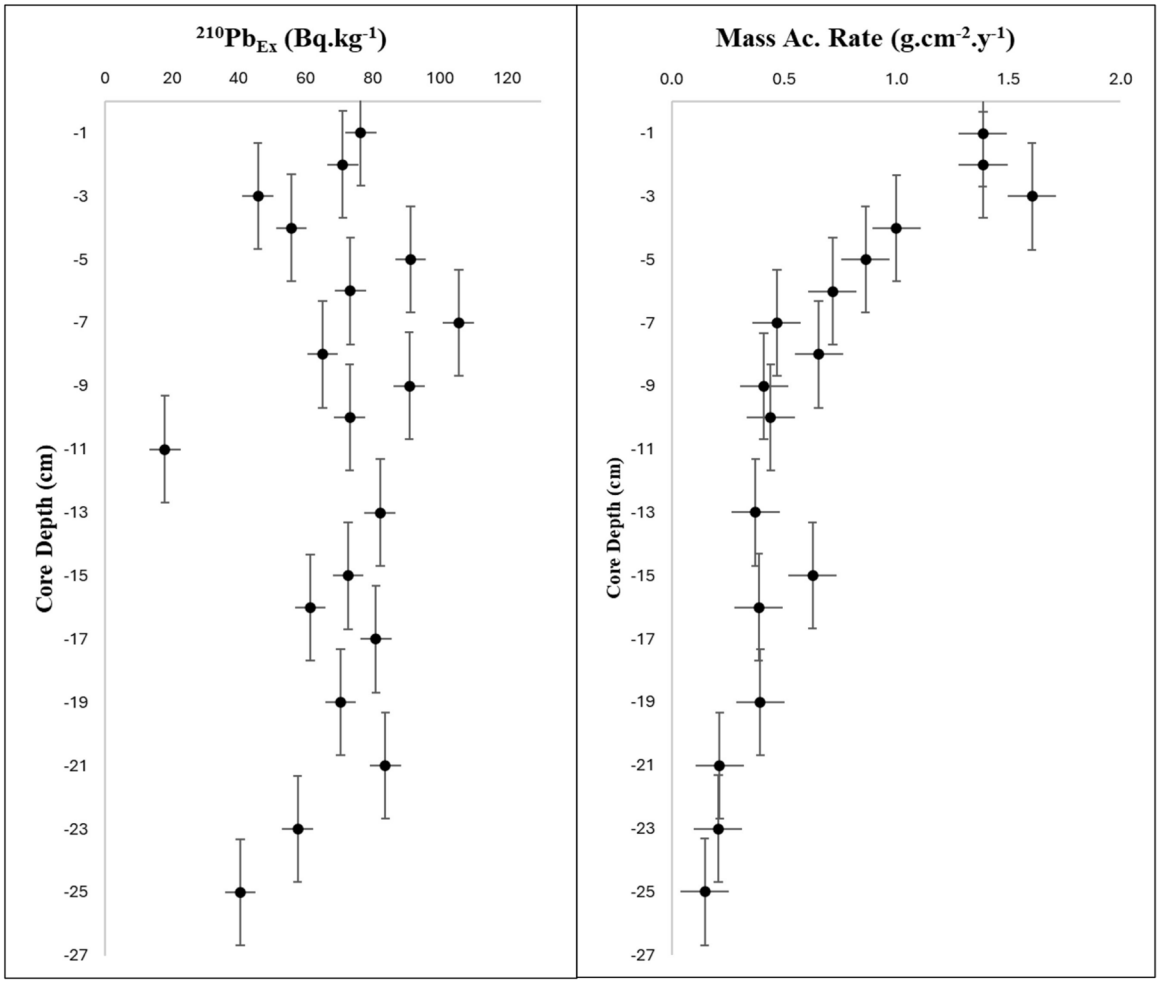


**Fig. 4** Vertical distribution of $^{210}Pb_{ex}$ activity and mass accumulation rates in core

CRS and CIC are mathematical models based on $^{210}$Pb. The half-life of naturally radioactive $^{210}$Pb is 22.30 years and it is accepted that a radionuclide loses its activity after 5 or 7 half-lives. Therefore, a chronology of approximately 150 years can be obtained using CRS and CIC models. This situation constitutes a potential limit in dating older sediments. Another important limitation in the use of CRS and CIC models is the good determination of the equilibrium depth at which the $^{210}$Pb concentration above the threshold decreases and reaches the $^{226}$Ra concentration. If the correct equilibrium depth cannot be determined, matching the $^{210}$Pb chronology with the time-marker $^{137}$Cs peaks will not be possible and a reliable chronology will not be obtained.

In present study, it was seen that Çınarcık Basin displays three different sediment accumulation trends over the last century, and average sedimentation rate is $0.25 \pm 0.01$ cm y$^{-1}$. Notably, the calculated $^{210}$Pb flux from the core exceeds the global atmospheric average, indicating significant external inputs likely stemming from surrounding catchments. These inputs are attributed to increased erosion associated with anthropogenic activities such as deforestation, rapid urbanization, and agricultural land use, particularly intensified after the 1980s. The sedimentation rate shows a marked increase starting in 1994, a period coinciding with major land development projects and accelerated coastal urban expansion in the Marmara region. Furthermore, the continued upward trend since 2011 may be linked to increasing frequency and intensity of extreme weather events, increasing catchment fluxes, as well as the ongoing development of urban infrastructure and maritime traffic in the region. These developments have likely exacerbated sediment input through both direct runoff and increased terrestrial material transport via rivers.

The increased sedimentation rates, and the proposed increase in catchment fluxes, can further exacerbate the ongoing hypoxia and mucilage problem in the Sea of Marmara [54, 55]. Particles carry eutrophication-enhancing elements such as nitrogen and phosphorus, as well as organic carbon, which altogether lead to further algal growth and nutrient loading in the system [56]. Recent hypoxia trends in

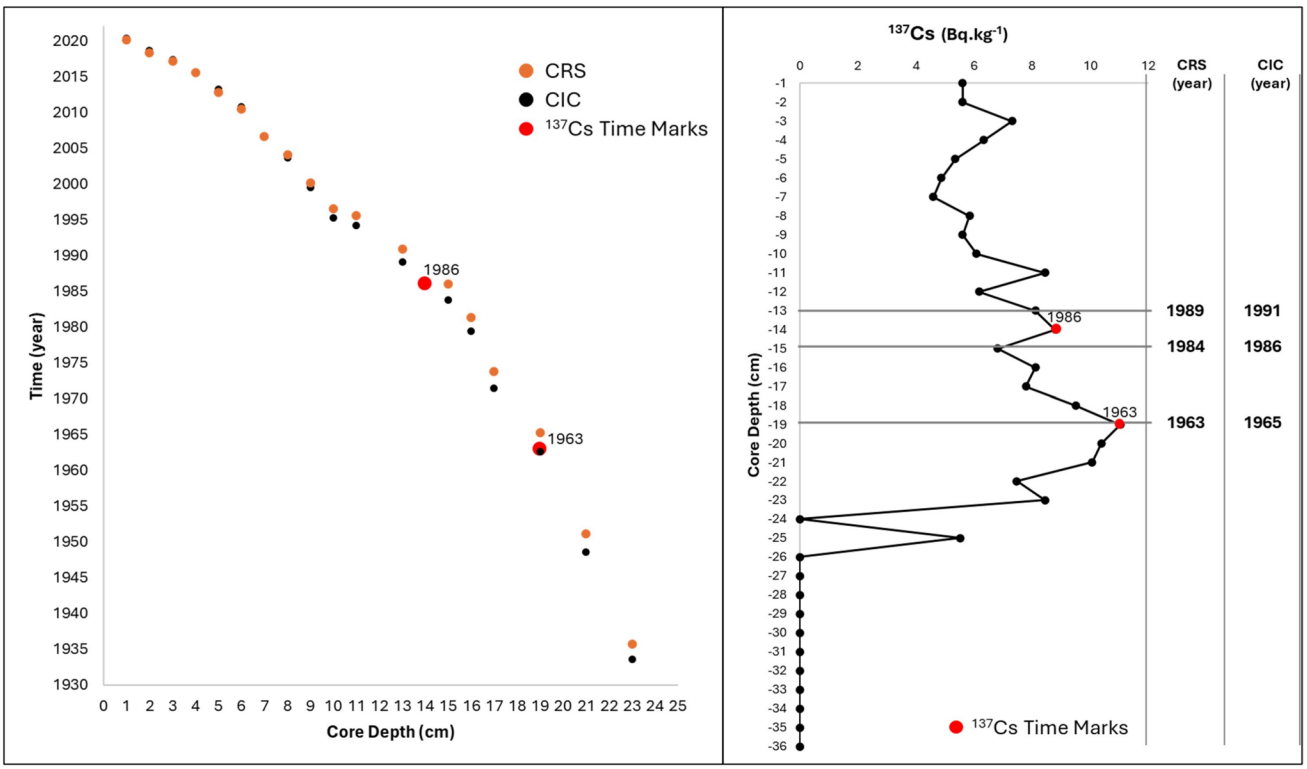


**Fig. 5** Sedimentation model results and $^{210}$Pb–$^{137}$Cs chronology

Çınarcık and İzmit bay may be very well linked to increased particle fluxes which can be captured in elevated sedimentation rates. Similar rate measurements will be needed in the near future from other locations in the Marmara coastal and deep basins to be able to test the idea of a basin-wide increased sedimentation, driven by broader socio-economic developments in the region.

The results contribute significantly to understanding the environmental history of the Çınarcık Basin, shedding light on both natural and human-induced factors influencing sedimentation and marine ecosystem changes over time. They also provide a basis for future research by enabling evaluation in conjunction with previous studies conducted in the region. While these findings offer valuable insights into localized sedimentation dynamics, they are intended to serve as a reference framework for assessing past and ongoing impacts within the Çınarcık Basin. Broader generalizations to the entire Sea of Marmara should be approached with caution, as regional variability requires more detailed, site-specific investigations. Therefore, this study should be considered a foundational step toward more comprehensive assessments that integrate the diverse environmental and anthropogenic dynamics across the Marmara region.

**Supplementary Information** The online version contains supplementary material available at https://doi.org/10.1007/s10967-025-10266-0.

**Acknowledgements** The data used in this paper were derived from İdris Koraltan's PhD thesis. The marine expedition that supported this study has been supported by DEKOSIM project (Centre for Marine Ecosystem and Climate Research, METU-IMS, Project Code BAP-08-11-DPT.2012K120880) and project MARMOD (funded by Ministry of Environment, Urbanization and Climate Change; coordinated by METU-IMS). We would like to express our sincere gratitude to Nimet Alımlı and Mertcan Esti for their assistance with fieldwork and thank to the crew and scientific party of R/V Bilim-2 for operational support during the expedition.

## Declarations

**Conflict of interest** No conflict of interest were disclosed. The authors declare that no competing financial interest could have appeared to influence the results reported in this paper.

## References

1. Çagatay MN, Özcan M, Güngör E (2004) Pore-water and sediment geochemistry in the Marmara Sea (Turkey): early diagenesis and diffusive fluxes. Geochem: Explor Environ Anal 4:213–225. https://doi.org/10.1144/1467-7873/04-202
2. Çağatay MN, Uçarkuş G (2019) Chapter 16: Morphotectonics of the Sea of Marmara: Basins and Highs on the North Anatolian Continental Transform Plate Boundary. In: Duarte JC (ed) Transform plate boundaries and fracture zones. Elsevier, pp 397–416
3. Öztürk İ (2021) Marmara Denizi ve Türk Boğazlar Sistemi. Turkish Marine Research Foundation (TUDAV), Ankara

4. Ozsoy E, Cagatay MN, Balkıs N, Balkıs N, Ozturk B (2016) The Sea of Marmara; Marine Biodiversity, Fisheries, Conservation and Governance. Turkish Marine Research Foundation (TUDAV), Istanbu, TÜRKİYE
5. TRDizin (2025) Ulusal Atıf Dizini. https://search.trdizin.gov.tr/tr/yayin/ara?q=marmara%20denizi&order=publicationYear-DESC&page=1&limit=20&facet-documentType=PROJECT. Accessed 5 Jan 2025
6. Görür N, Cagatay MN, Sakinc M, Sümengen M, Sentürk K, Yaltirak C, Tchapalyga A (1997) Origin of the Sea of Marmara as deduced from Neogene to Quaternary paleogeographic evolution of its frame. Int Geol Rev 39:342–352. https://doi.org/10.1080/00206819709465276
7. Öztürk K, Yaltirak C, Alpar B (2009) The relationship between the tectonic setting of the Lake İznik Basin and the Middle Strand of the North Anatolian Fault. Turk J Earth Sci. https://doi.org/10.3906/yer-0803-4
8. Sengör AMC (1979) The North Anatolian transform fault: its age, offset and tectonic significance. JGS 136:269–282. https://doi.org/10.1144/gsjgs.136.3.0269
9. Vardar D, Alp H, Demirel S, Vardar H, Alpar B (2021) Seismic stratigraphy of the north-western Sea of Marmara shelf along the North Anatolian Fault system. Ann Geophys. https://doi.org/10.4401/ag-8591
10. Biltekin D, Eriş KK, Çağatay MN, Henry P, Yakupoğlu N (2023) New records of vegetation and climate changes in the Sea of Marmara during the Marine Isotope Stages 3, 4 and 5 (a-c). Quatern Int 667:1–18. https://doi.org/10.1016/j.quaint.2023.06.005
11. Evans G, Erten H, Alavi SN, Von Gunten HR, Ergin M (1989) Superficial deep-water sediments of the Eastern Marmara Basin. Geo-Mar Lett 9:27–36. https://doi.org/10.1007/BF02262815
12. Gözel F, Belivermiş M, Sezer N, Kurt MA, Sıkdokur E, Kılıç Ö (2022) Chronology of trace elements and radionuclides using sediment cores in Golden Horn Estuary, Sea of Marmara. Environ Pollut 315:120359. https://doi.org/10.1016/j.envpol.2022.120359
13. Sabuncu A, Eriş KK, Demirbağ E, Vardar D (2024) Pre-Holocene Morphobathymetry of Sea of Marmara (SoM) Sedimentary Basins: A Case Study With Precise Correlations Developed by Sediment Cores and HR Seismic Profiles. Copernicus Meetings
14. Vidal L, Ménot G, Joly C, Bruneton H, Rostek F, Çağatay MN, Major C, Bard E (2010) Hydrology in the Sea of Marmara during the last 23 ka: Implications for timing of Black Sea connections and sapropel deposition. Paleoceanography 25:. https://doi.org/10.1029/2009PA001735
15. Öztürk H, Alkan G (2021) Türkiye'nin Ekstrem Deniz Ortamları. Türk Deniz Araştırmaları Vakfı (TÜDAV), İstanbul, Türkiye
16. Yücel S, Ünsal Özgüvenç T, Çağlar N (2022) Marmara Denizi Çinarcik Çukuru'nda Anoksik ve Suboksik Koşullarin Değerlendirilmesi. pp 65–66
17. Sarı E, Çağatay MN (2006) Turbidites and their association with past earthquakes in the deep Çınarcık Basin of the Marmara Sea. Geo-Mar Lett 26:69–76. https://doi.org/10.1007/s00367-006-0017-3
18. Hajdas I, Ascough P, Garnett MH, Fallon SJ, Pearson CL, Quarta G, Spalding KL, Yamaguchi H, Yoneda M (2021) Radiocarbon dating. Nat Rev Methods Primers 1:1–26. https://doi.org/10.1038/s43586-021-00058-7
19. Pilcher JR (2005) Radiocarbon dating and environmental radiocarbon studies. In: Global change in the holocene. Routledge
20. Stuiver M, Polach HA (1977) Discussion reporting of 14C data. Radiocarbon 19:355–363. https://doi.org/10.1017/S0033822200003672
21. Corbett DR, Walsh J p. (2015) 210Lead and 137Cesium. In: Handbook of sea-level research. Wiley, pp 361–372
22. He Q, Walling DE (1996) Use of fallout Pb-210 measurements to investigate longer-term rates and patterns of overbank sediment deposition on the floodplains of lowland rivers. Earth Surf Process Landf 21:141–154. https://doi.org/10.1002/(SICI)1096-9837(199602)21:2%3c141::AID-ESP572%3e3.0.CO;2-9
23. Saravana Kumar U, Navada SV, Rao SM, RmP N, Kumar B, Krishnamoorthy TM, Jha SK, Shukla VK (1999) Determination of recent sedimentation rates and pattern in Lake Naini, India by 210Pb and 137Cs dating techniques. Appl Radiat Isotopes 51:97–105. https://doi.org/10.1016/S0969-8043(98)00148-1
24. Lu X, Matsumoto E (2005) Recent sedimentation rates derived from 210Pb and 137Cs methods in Ise Bay, Japan. Estuar Coast Shelf Sci 65:83–93. https://doi.org/10.1016/j.ecss.2005.05.009
25. Lu X (2004) Application of the Weibull extrapolation to $^{137}$Cs geochronology in Tokyo Bay and Ise Bay, Japan. J Environ Radioactiv 73:169–181. https://doi.org/10.1016/j.jenvrad.2003.08.009
26. Ritchie JC, McHenry JR (1990) Application of radioactive fallout cesium-137 for measuring soil erosion and sediment accumulation rates and patterns: a review. J Environ Qual 19:215–233. https://doi.org/10.2134/jeq1990.00472425001900020006x
27. Abril JM (2022) On the use of 210Pb-based records of sedimentation rates and activity concentrations for tracking past environmental changes. J Environ Radioactiv 244–245:106823. https://doi.org/10.1016/j.jenvrad.2022.106823
28. Appleby PG, Oldfield F (1978) The calculation of lead-210 dates assuming a constant rate of supply of unsupported 210Pb to the sediment. CATENA 5:1–8. https://doi.org/10.1016/S0341-8162(78)80002-2
29. Baskaran M (2011) Po-210 and Pb-210 as atmospheric tracers and global atmospheric Pb-210 fallout: a review. J Environ Radioactiv 102:500–513. https://doi.org/10.1016/j.jenvrad.2010.10.007
30. Bunke D, Leipe T, Moros M, Morys C, Tauber F, Virtasalo JJ, Forster S, Arz HW (2019) Natural and anthropogenic sediment mixing processes in the south-western Baltic Sea. Front Mar Sci. https://doi.org/10.3389/fmars.2019.00677
31. Owens PN (2020) Soil erosion and sediment dynamics in the Anthropocene: a review of human impacts during a period of rapid global environmental change. J Soils Sediments 20:4115–4143. https://doi.org/10.1007/s11368-020-02815-9
32. Walling DE, He Q (1999) Using Fallout lead-210 measurements to estimate soil erosion on cultivated land. Soil Sci Soc Am J 63:1404–1412. https://doi.org/10.2136/sssaj1999.6351404x
33. Du M, Hu T, Liu W, Shi M, Li P, Mao Y, Liu L, Xing X, Qi S (2024) Chronological evaluation of polycyclic aromatic hydrocarbons in sediments of Tangxun Lake in central China and impacts of human activities. Environ Sci Pollut Res 31:54887–54904. https://doi.org/10.1007/s11356-024-34816-3
34. Kuzmenkova N, Rozhkova A, Egorin A, Tokar E, Grabenko E, Shi K, Petrov V, Kalmykov S, Hou X (2023) Analysis of sedimentation processes in Lake Khanka (Xingkaihu) and Amur Bay using 137Cs and 210Pbex tracers. J Radioanal Nucl Chem 332:959–971. https://doi.org/10.1007/s10967-023-08813-8
35. Chen J, Zhang X, Navas A, Wen A, Wang X, Zhang R (2020) A study on a $^{210}Pb_{ex}$ accumulation-decay model for dating moraine soils to trace glacier retreat time. J Environ Radioactiv 212:106124. https://doi.org/10.1016/j.jenvrad.2019.106124
36. Sanchez-Cabeza JA, Ruiz-Fernández AC (2012) 210Pb sediment radiochronology: an integrated formulation and classification of dating models. Geochim Cosmochim Acta 82:183–200. https://doi.org/10.1016/j.gca.2010.12.024
37. Sert I, Yener G, Ozel E, Pekcetinoz B, Eftelioglu M, Ugur Gorgun A (2012) Estimation of sediment accumulation rates using naturally occuring 210Pb models in Gülbahçe Bay, Aegean Sea, Turkey. J Environ Radioactiv 107:1–12. https://doi.org/10.1016/j.jenvrad.2011.11.002
38. Gökmen A, Yıldız M, Erten HN, Salihoğlu İ (1996) Dating the Sea of Marmara sediments by a uniform mixing model. J Environ Radioact 33(1):91–104

39. Ergin M, Bodur Mn, Yıldız M, Ediger D, Ediger V, Yemenicioğlu S, Yücesoy F (1994) Sedimentation rates in the Sea of Marmara: a comparison of results based on organic carbon-primary productivity and $^{210}$Pb dating. Cont Shelf Res 14(2):1371–1387
40. Jedari C, Palomino A, Cyr H, Drumm E, Boles D (2017) Grain and Floc Size Distribution Analysis of Fine Coal Refuse Slurry. Seoul, Korea, pp 403–406
41. Sert I (2018) Sediment chronology and historical evolution of heavy metal contamination in terms of pollution index in Turkish coast, north Aegean Sea. J Radioanal Nucl Chem 318:1805–1819. https://doi.org/10.1007/s10967-018-6043-6
42. Athy LF (1930) Density, porosity, and compaction of sedimentary rocks. AAPG Bull 14:1–24
43. Begy R, Cosma C, Timar A (2009) Recent changes in Red Lake (Romania) sedimentation rate determined from depth profiles of 210Pb and 137Cs radioisotopes. J Environ Radioactiv 100:644–648. https://doi.org/10.1016/j.jenvrad.2009.05.005
44. Klump JV, Paddock R, Remsen CC, Fitzgerald S, Boraas M, Anderson P (1989) Variations in sediment accumulation rates and the flux of labile organic matter in eastern Lake Superior basins. J Great Lakes Res 15:104–122. https://doi.org/10.1016/S0380-1330(89)71465-9
45. Sert I, Ozel FE, Yaprak G, Eftelioglu M (2016) Determination of the latest sediment accumulation rates and pattern by performing 210Pb models and 137Cs technique in the Lake Bafa, Mugla, Turkey. J Radioanal Nucl Chem 307:313–323. https://doi.org/10.1007/s10967-015-4234-y
46. Kumar A, Rout S, Karpe R, Mishra MK, Narayanan U, Singhal RK, Ravi PM, Tripathi RM (2015) Inventory, fluxes and residence times from the depth profiles of naturally occurring 210Pb in marine sediments of Mumbai Harbor Bay. Environ Earth Sci 73:4019–4031. https://doi.org/10.1007/s12665-014-3687-6
47. Sert I, Eftelioglu M, Ozel FE (2017) Historical evolution of heavy metal pollution and recent records in Lake Karagöl sediment cores using 210Pb models, western Turkey. J Radioanal Nucl Chem 314:2155–2169. https://doi.org/10.1007/s10967-017-5627-x
48. Yalçın B, Artüz ML, Pavlidou A, Çubuk S, Dassenakis M (2017) Nutrient dynamics and eutrophication in the Sea of Marmara: data from recent oceanographic research. Sci Total Environ 601–602:405–424. https://doi.org/10.1016/j.scitotenv.2017.05.179
49. Demirel N, Akoglu E, Ulman A, Ertor-Akyazi P, Gül G, Bedikoğlu D, Yıldız T, Yilmaz IN (2023) Uncovering ecological regime shifts in the Sea of Marmara and reconsidering management strategies. Mar Environ Res 183:105794. https://doi.org/10.1016/j.marenvres.2022.105794
50. Balkıs N, Çağatay MN (2001) Factors controlling metal distributions in the surface sediments of the Erdek Bay, Sea of Marmara, Turkey. Environ Int 27:1–13. https://doi.org/10.1016/S0160-4120(01)00044-7
51. Basdurak BN (2023) Climate change impacts on river discharge to the Sea of Marmara. Front Mar Sci. https://doi.org/10.3389/fmars.2023.1278136
52. Hiscott RN, Aksu AE, Yaltırak C (2021) The uppermost Pleistocene-Holocene mud drape across the Marmara Sea: quantification of detrital supply from southern Marmara rivers. Sediment Geol 415:105851. https://doi.org/10.1016/j.sedgeo.2021.105851
53. Karageorgis AP, Kaberi H, Price NB, Muir GKP, Pates JM, Lykousis V (2005) Chemical composition of short sediment cores from Thermaikos Gulf (Eastern Mediterranean): sediment accumulation rates, trawling and winnowing effects. Cont Shelf Res 25:2456–2475. https://doi.org/10.1016/j.csr.2005.08.006
54. Belivermiş M, Kılıç Ö, Sezer N, Sıkdokur E, Güngör ND, Altuğ G (2021) Microplastic inventory in sediment profile: a case study of Golden Horn Estuary, Sea of Marmara. Mar Pollut Bull 173:113117. https://doi.org/10.1016/j.marpolbul.2021.113117
55. Akın S, Tuğrul S, others (2021) The sea snot outbreak in the Sea of Marmara: Biogeochemical transformations of the sea, modern-day pressures and a roadmap for the way forward. Ecology of the Marmara Sea: Formation and Interactions of Marine Mucilage, and Recommendations for Solutions (eds, Öztürk, İ, Şeker, M) Turkish Academy of Sciences, Ankara, Turkey 249–267
56. Akçay İ, Yücel M (2023) Distinct patterns of sedimentary phosphorus fractionation and mobilization in the seafloor of the Black Sea, Marmara Sea and Mediterranean Sea. Sci Total Environ 863:160936. https://doi.org/10.1016/j.scitotenv.2022.160936